

Electrochemical and Morphological Analysis of Mercury Sulphide for Capacitance Behaviour

Peeyush Phogat¹, Jahanvi Thakur¹, Shreya¹, Ranjana Jha¹ and Sukhvir Singh¹

¹Research Lab for Energy Systems, Department of Physics, Netaji Subhas University of Technology, New Delhi, India

ABSTRACT

Electrochemical capacitors (ECs) are an important component of modern energy storage due to their fast charge-discharge kinetics, high power density, and long operating life. This work investigates the electrochemical behaviour and morphological characteristics of mercury sulfide (HgS) electrodes, using cyclic voltammetry and scanning electron microscopy for a thorough analysis. HgS was produced using a single-step hydrothermal method. X-ray diffraction revealed the presence of single-phase HgS. The W-H and S-S plots determine the crystallite size. UV-Vis spectroscopy investigation indicates absorption in both UV and visible regions, with an optical energy band gap of 0.79 eV. FESEM detected nano-polyhedral particles. EDS analysis using FESEM revealed the presence of mercury and sulfur. The Nyquist plot and cyclic voltammetry showed capacitive behavior, indicating compatibility with batteries and supercapacitors. The study thoroughly investigates HgS electrodes to identify crucial elements influencing capacitance performance, such as electrode shape, surface area, and material composition. The findings highlight HgS's potential as an effective electrode material and provide insights into its use in developing EC technology. This study contributes to the ongoing development of energy storage systems by linking fundamental electrochemical principles with comprehensive morphological characterization, paving the way for long-lasting and efficient capacitive devices.

INTRODUCTION

In the realm of energy storage and conversion technologies, electrochemical capacitors (ECs), also known as supercapacitors or ultracapacitors, have emerged as promising alternatives to traditional energy storage devices such as batteries [1],[2] Unlike batteries, which store energy through chemical reactions, ECs do it electrostatically at the electrode-electrolyte contact [3],[4]. This mechanism enables ECs to provide rapid charge and discharge cycles, high power density, and long cycle life [5] making them excellent for applications that require frequent and rapid energy transfers, such as hybrid automobiles, solar power plants, and portable devices [6], [7].

Electrochemical capacitors offer numerous distinct benefits over conventional batteries. They have a high-power density, which allows them to deliver bursts of energy quickly and efficiently. This feature is especially useful in applications requiring rapid energy delivery, such as regenerative braking in automobiles or peak power shaving in electrical grids [8],[9]. Furthermore, ECs often maintain their performance over long cycles, with low degradation even after hundreds of thousands or millions of charge-discharge cycles [10],[11]. This longevity translates into lower maintenance costs and a longer operational lifespan compared to batteries, making ECs economically appealing for both industrial and consumer applications [12], [13].

Another significant feature of ECs is their capacity to function well across a wide temperature range, from sub-zero to high thermal conditions [14]. This robust thermal performance ensures reliable operation in various climatic conditions, making them ideal for outdoor and automotive applications. Moreover, electrochemical capacitors are frequently built using environmentally friendly materials and do not rely on harmful compounds or heavy metals found in typical battery chemistries [15],[16]. This feature not only reduces their environmental impact but also simplifies end-of-life disposal and recycling, aligning with sustainable energy storage practices.

The pursuit of improved performance and efficiency in ECs has prompted continuous research into novel electrode materials, with mercury sulphide (HgS) emerging as a viable candidate. HgS, known for its semiconductor properties and chemical durability, offers exciting opportunities to enhance capacitive behaviour in energy storage applications. The electrochemical performance of HgS is heavily influenced by its interaction with electrolytes as well as its morphological features, such as surface area and particle size distribution. Understanding these interactions requires extensive study and characterization to fully realize HgS potential in advancing electrochemical capacitor technology.

This research investigates the electrochemical and morphological properties of mercury sulphide electrodes using modern analytical techniques such as cyclic voltammetry and scanning electron microscopy. The study aims to help optimize and build next-generation electrochemical capacitors by

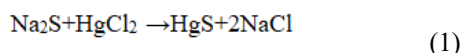
elucidating the links between electrode structure, surface characteristics, and electrochemical performance. Ultimately, by combining the benefits of ECs with the unique features of mercury sulphide, this research seeks to promote innovation in energy storage technologies, resulting in more efficient, sustainable, and diverse solutions.

EXPERIMENTAL SECTION

Synthesis of Mercury Sulphide

To begin, make a 0.1M solution of sodium sulphide (1.5g) in 35ml of deionized water and stir for 1 hour. Prepare another solution of 0.3M mercury chloride (0.25g) by stirring it in 20ml of deionized water at room temperature for 1 hour. After an hour, add the sodium sulphide solution to the mercury chloride solution dropwise at 5-minute intervals. Allow this solution to stand for 1 hour, stirring constantly. After an hour, transfer the final solution into a 100ml Teflon-lined stainless-steel autoclave, seal it, and treat it at 180°C for 24 hours. After 24 hours, let it cool.

Next, centrifuge the precipitate and wash it several times with deionized water and ethanol. Then, dry the precipitate in a vacuum oven at 70°C overnight. The following day, crush the samples into a fine powder.



Deposition of Thin Film for Working Electrodes

First, the FTO substrate must be thoroughly cleaned to ensure it is free of contaminants. This cleaning process involves sequentially sonicating the substrate in acetone, isopropanol, and deionized water for 10 minutes each [17]. After cleaning, the substrate is dried with nitrogen gas and baked at 100°C for 10 minutes to remove any residual moisture.

Next, prepare the HgS solution as previously described, ensuring it is well-mixed and free of particulate matter. If necessary, filter the solution using a 0.45-micron syringe filter to remove impurities. For the spin coating process, place the clean FTO substrate onto the spin coater chuck and secure it with a vacuum to keep it stationary. Dispense a measured amount of the HgS solution onto the centre of the substrate, then set the spin coater to rotate at 1000 rpm for 30 seconds. The centrifugal force will evenly spread the solution across the substrate surface, forming a uniform thin film.

After spin coating, carefully transfer the coated substrate to a hot plate or oven set at 70°C. Allow the film to dry for 10-15 minutes to evaporate any remaining solvent and promote adhesion of the HgS layer to the FTO substrate, helping to form a continuous and uniform thin film [18].

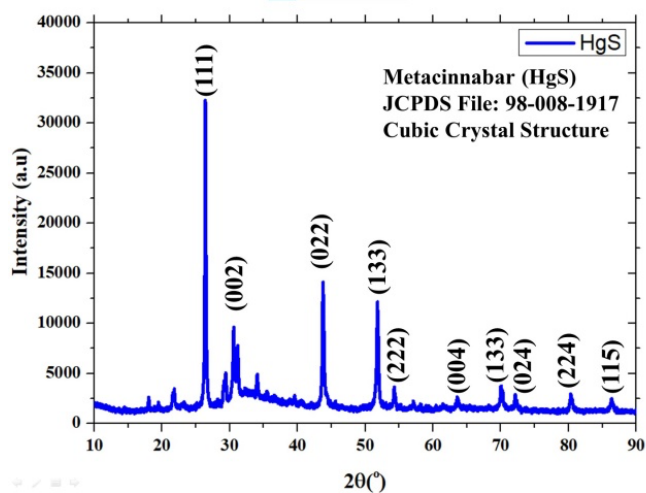
Electrochemical Study

In this study, we employed cyclic voltammetry (CV) and potentiostatic electrochemical impedance spectroscopy (PEIS) using a Biologic SP-240 three-electrode system to investigate the electrochemical properties of as-synthesized samples intended for capacitance and supercapacitance applications [19]. The experimental setup included a reference electrode (Ag|AgCl), a platinum counter electrode, and the synthesized thin film as the working electrode. The analysis employed an electrolyte containing a 0.5 M LiI solution.

RESULTS AND DISCUSSION

Structural Analysis

The as-synthesized samples were examined using a Cu K α X-ray diffractometer in Bragg-Brentano geometry ($\lambda = 1.54 \text{ \AA}$), scanning from 10° to 90° in 2 θ . Figure 1(a) depicts the resulting X-ray diffraction patterns, which show unique peaks that correspond to specific crystalline phase. The analysis of the patterns revealed the presence of HgS peaks, which corresponded to the JCPDS file 98-008-1917. The reflections along the (111), (002), (022), (133), (222), (004), (133), (024), (224), and (115) planes indicate the formation of a cubic HgS crystal structure, as illustrated in Fig. 1(b). This cubic structure is characteristic of the sphalerite phase of HgS [20], [21]. The sharp and well-defined peaks suggest that the synthesized HgS nanocrystals are of high crystalline quality, with minimal impurities or secondary phases. These results confirm the successful synthesis of HgS with the desired crystal structure, which is crucial for its potential applications in various fields.



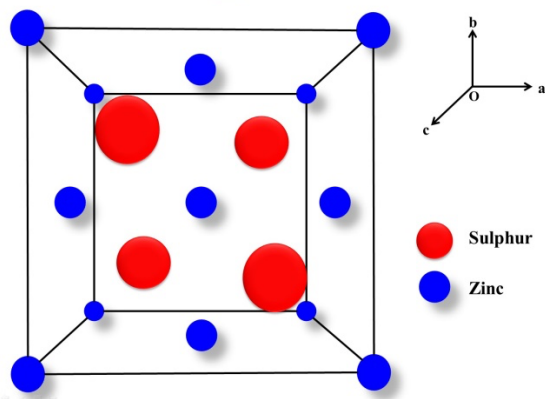


Figure 1. (a) XRD pattern for as-synthesized materials with their respective (hkl) indices on the top of the peaks, (b) 3D structures.

The lattice characteristics of the constituent phases of nanocomposites have a considerable influence on their formation. Thus, the conventional cubic equations between d spacing and lattice parameter were used to calculate the lattice parameters of HgS phases in each composite sample. Table 1 summarizes the computed lattice parameter values and compares them to the conventional JCPDS values. The as-synthesized samples lattice parameters differed slightly from conventional JCPDS values. This demonstrates the presence of strain in the material. The Debye Scherrer (D-S) equation was used to determine the average crystallite size of the critical for improving light absorption and reducing reflection losses [22]. Anti-reflective coatings with spec synthesized samples, which was 46 nm, as shown in table 2. The D-S equation assumes isotropic crystallite characteristics with no strain in the material [23].

The as-synthesized samples were analyzed using the Williamson-Hall (W-H) plot approach, which assessed both microstructural strain and crystallite size while taking into consideration isotropic strain effects across the whole X-ray diffraction (XRD) spectrum [24]. Figure 2(a) depicts the samples W-H plots, which show the slope (related to crystallite size) and intercept (related to strain) values obtained using linear regression analysis. Table 2 summarizes the calculated crystallite size and strain based on the slope and intercept compared to the traditional W-H equation.

The Size-Strain (S-S) analysis uses Gaussian and Lorentzian functions to evaluate strain and crystallite size, taking into consideration low contributions from high 2θ peaks [25]. Figure 2(b) illustrates this method, which uses Rietveld refinement to correct Full Width Half Maximums (FWHMs) for instrumental broadening. Table 2 summarizes crystallite sizes and stresses obtained using various analytical methods, highlighting the effectiveness of S-S plots in capturing precise structural information.

Table 1. Lattice parameter calculated for HgS.

	a	b	c
Lattice parameter of as synthesized HgS (Å)	5.84	5.84	5.84
Lattice parameters from JCPDS 98-008-1917	5.85	5.85	5.85

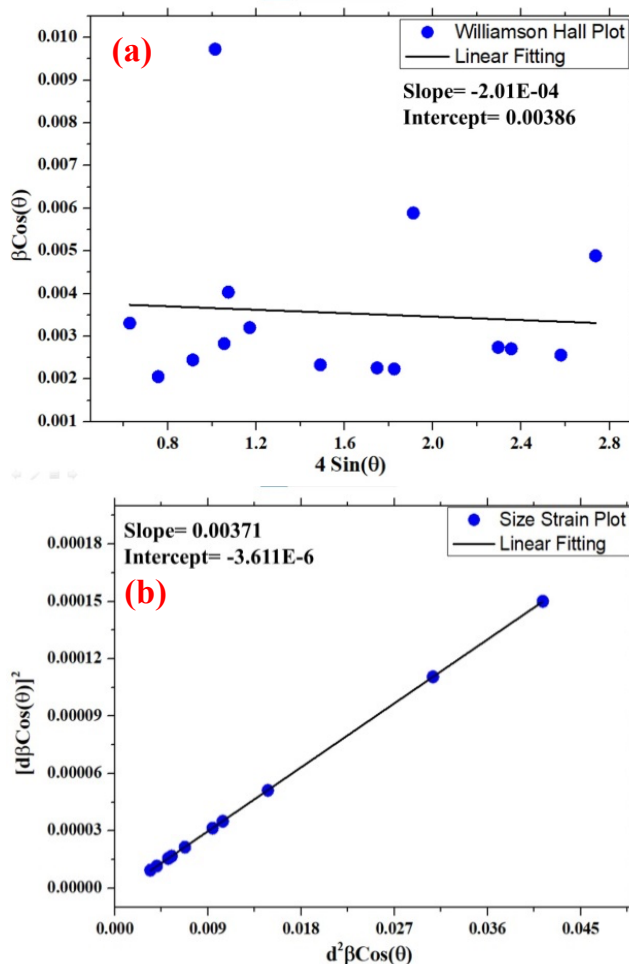


Figure 2. (a) Williamson Hall plot, (b) Size Strain plot of as-synthesized HgS with their respective slope and intercept.

Table 2. Crystallite size of HgS as calculated by Debye Scherrer equation, W–H plots and S–S plots.

Parameter	Debye Scherrer	Williamson Hall	Size Strain
Crystallite size(nm)	46	35	37
strain	-	-2.0 E-04	3.8 E-03

Optical Analysis

Optical analysis is critical for understanding the properties of mercury sulphide (HgS). UV-Vis spectroscopy is an optical

method that provides vital insights into its electronic structure and optical properties. UV-Vis spectroscopy was utilized to investigate the optical properties of the nanocomposites as they were formed. The analysis involved determining absorbance, optical band gap, and illustrating the sample absorbance spectra, which revealed absorption in both the UV and visible ranges. The absorbance peaks were found at wavelengths of 331, 373, 416, 534, 704, and 847 nm, with the maximum absorption at 847 nm as shown in figure 3(a).

The sample band gap analysis was carried out using Tauc plots [26], a well-known method for finding optical band gaps in materials. Absorbance data was examined using Tauc's method and Menth's equation to create plots, allowing for the measurement of the sample band gap, which was found to be 0.79 eV, as shown in Figure 3(b).

This low band gap value suggests that HgS nanocomposites can effectively absorb lower energy photons, making them suitable for applications in optoelectronic devices such as photodetectors and solar cells [27]. The broad absorbance spectrum, covering both the UV and visible ranges, indicates that the HgS nanocomposites can be utilized in a variety of photonic applications, including UV protection and visible light harvesting. Additionally, the distinct absorbance peaks at multiple wavelengths imply the presence of different electronic transitions and possible quantum confinement effects in the nanocomposites.

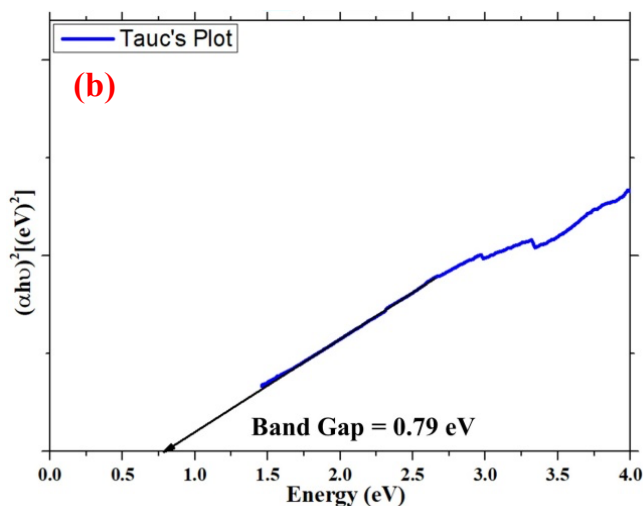
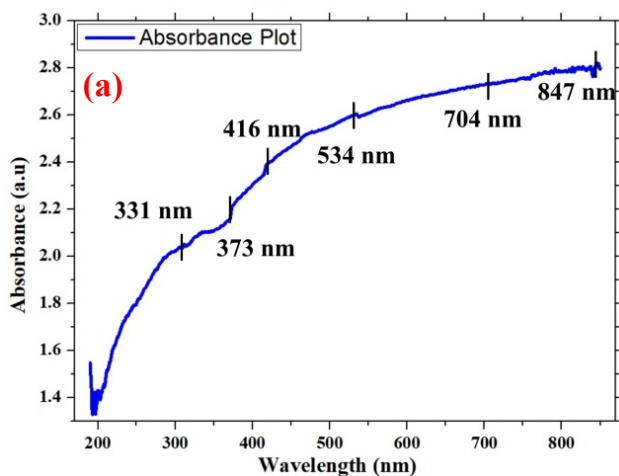


Figure 3. (a) Absorbance spectra, (b) Tauc plot for as synthesized HgS with their respective band gaps.

Surface Morphological Analysis

Field emission scanning electron microscopy (FESEM) was used to examine the morphology of HgS, resulting in increased resolution, improved surface contrast, greater depth of field, and enhanced operational versatility. The morphology of HgS indicates a polyhedral shape and size with irregularities (Fig. 4(a) (b)). These irregularities can improve ion transit and increase the accessibility of active sites, enabling supercapacitors to offer high power densities. They serve as anchor points for active materials, minimize particle aggregation, and enhance structural integrity during charge-discharge cycles, contributing to increased cycle life and performance. They also improve the effective surface area, thus increasing the amount of stored charge per unit volume, resulting in higher energy densities.

The agglomerates present feature rougher surfaces and more complex geometries, which may enhance the effective surface area available for charge storage in supercapacitors. The porous nature of the agglomerates allows for efficient ion diffusion within the electrode material, facilitating faster charge/discharge speeds. Additionally, the mechanical stability of the agglomerates may contribute to enhanced structural integrity of the electrode material during cycling, resulting in increased long-term performance and durability of supercapacitors.

The elemental composition of the samples was determined by Energy Dispersive X-ray Spectroscopy (EDX) analysis, as shown in (Fig. 4c). The EDX spectra clearly indicated the presence of mercury (Hg) and sulfur (S) in the substance. This quantitative analysis confirms the elemental elements of the synthesized samples, providing critical information about their chemical composition.

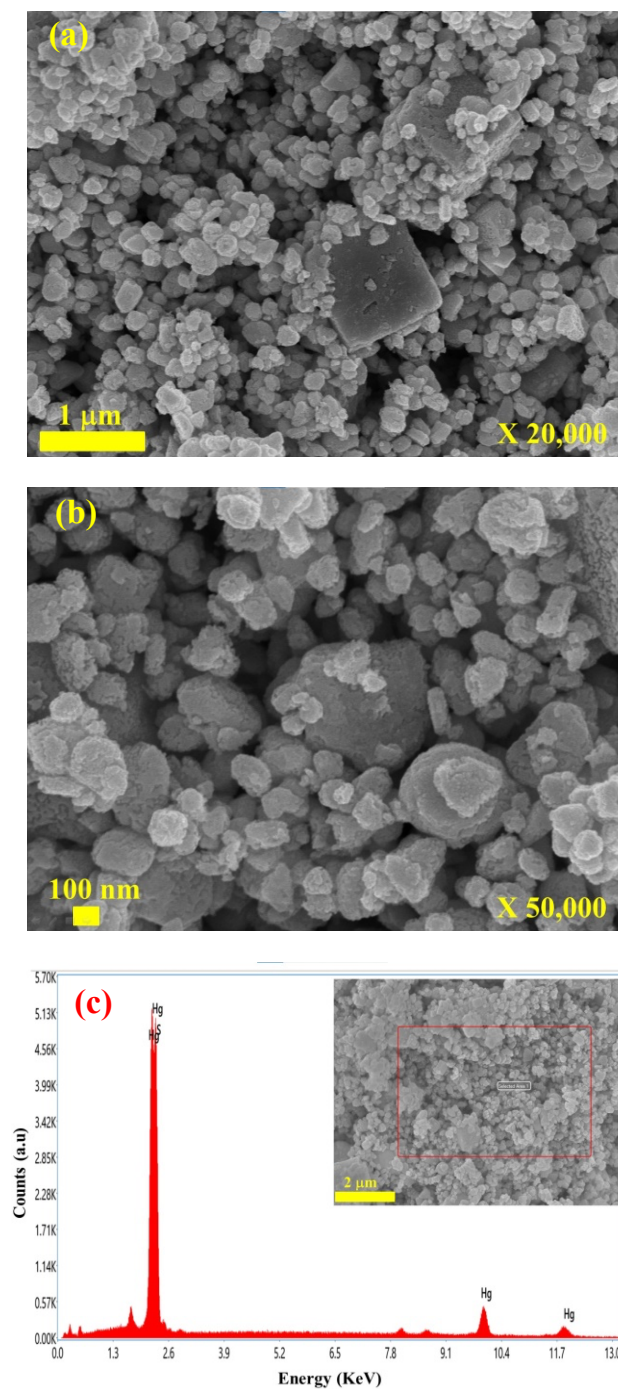


Figure 4. FESEM images of the samples HgS at different magnifications (a) X 50,000, (b) X20,000, (c) EDX pattern for inset selected area.

Cyclic Voltammetry

The CV curves of HgS reveal two distinct peaks in both forward and reverse scans, indicating a characteristic two-step redox process inherent to the material. As scan rates increase, the peak currents also rise while the peak separation widens, consistent with typical electrochemical behaviour. This behaviour

signifies HgS undergoes a complex electrochemical conversion during cycling [28].

In capacitor applications, ideal materials typically exhibit rectangular-shaped CV curves with minimal peak separation, indicative of rapid and reversible charge storage and discharge [29]. Although the CV curves of HgS in Figure 5 deviate somewhat from this ideal form, they do display promising characteristics for capacitor utilization. For effective capacitor performance, materials must possess several critical properties. Firstly, high specific capacitance is crucial, as it determines the amount of charge that can be stored per unit mass of material. Secondly, fast charge and discharge rates, governed by the kinetics of electrode reactions, are essential for responsive energy storage applications. Lastly, good cyclic stability is paramount—the material should endure numerous charge/discharge cycles without significant degradation [30].

HgS exhibits potential in these regards, showcasing a distinctive electrochemical behaviour suitable for capacitor applications despite the observed CV curve characteristics. Its ability to undergo a two-step redox process, albeit with some peak separation, suggests it can facilitate efficient charge storage and release. Further optimization and understanding of its electrochemical properties could enhance its performance and broaden its applicability in energy storage technologies.

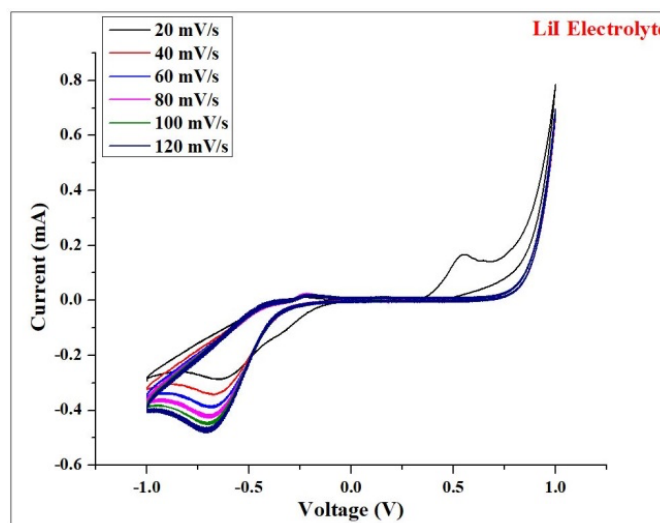


Figure 5. Cyclic Voltammetry of HgS in a LiI electrolyte.

Nyquist Plot

The Nyquist plot serves as a pivotal tool in electrochemical impedance spectroscopy (EIS), offering deep insights into the impedance characteristics of materials such as HgS. When examining the Nyquist plot for HgS, a distinctive semicircle-like shape typically emerges, mirroring the electrochemical behaviour akin to a Randle's circuit [31].

In the framework of Randle's circuit [32], which models the impedance of an electrochemical cell, the impedance Z can be expressed as

$$Z = R_1 + \frac{1}{\frac{1}{R_2} + j\omega C_2} \quad (2)$$

where R_1 denotes the solution resistance, R_2 represents the charge transfer resistance, C_2 signifies the capacitance, j stands for the imaginary unit, and ω denotes angular frequency. With specific values like $R_1=2.045 \times 10^6$ Ohm, $R_2=56.28$ Ohm and $C_2=24.33 \times 10^{-6}$ F, the behaviour of this configuration can be elucidated.

Analyzing the Nyquist plot reveals a semicircle, indicative of HgS's impedance profile resembling that of a Randle's circuit [33]. This semicircular shape signifies a blend of R_2 and C_2 influencing the impedance response, particularly at intermediate frequencies.

The Randle's circuit model underscores that at higher frequencies, the impedance primarily hinges on $2 + \frac{1}{j\omega C_2}$, highlighting the capacitive nature of HgS. This configuration underscores how C_2 facilitates efficient charge storage and discharge processes, essential for capacitive devices requiring rapid energy management.

The presence of a semicircle in the Nyquist plot and the configuration $R_1/(R_2+C_2)$ signifies robust charging capabilities, emphasizing HgS's suitability for applications demanding high efficiency in energy storage and release [34]. The semicircle-like Nyquist plot of HgS, reminiscent of a Randle's circuit characterized by parameters R_1 , R_2 , and C_2 , underscores its capacitive prowess [35]. This configuration not only supports efficient charging dynamics but also enhances HgS's potential across various capacitive device applications as illustrative in Figure 6.

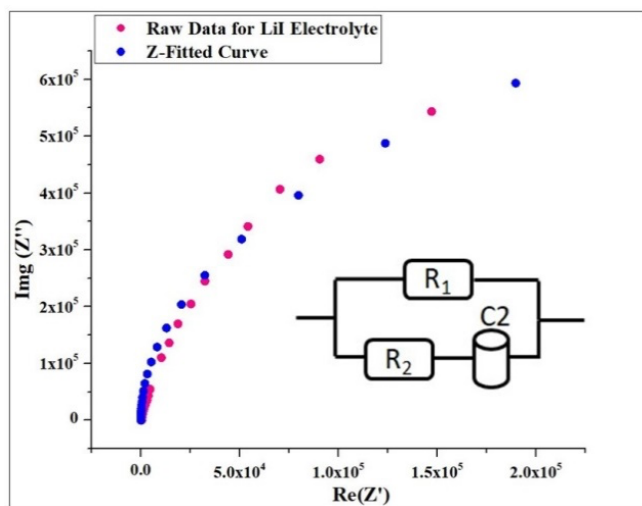


Figure 6. Nyquist Plot of HgS in a LiI electrolyte.

CONCLUSION

This study shows the high potential of mercury sulfide (HgS) as an electrode material for electrochemical capacitors. HgS was successfully synthesized using a hydrothermal technique, and X-ray diffraction confirmed its high crystalline quality, which is required for energy storage applications. Electrochemical investigations, such as cyclic voltammetry and electrochemical impedance spectroscopy, revealed that HgS had a positive capacitive characteristic. These findings suggest that HgS is ideal for high-power applications due to its effective charge-discharge kinetics and low resistance, which are critical for the rapid cycling requirements of ECs.

Furthermore, UV-Vis spectroscopy demonstrated that HgS has a broad absorption spectrum that includes both UV and visible wavelengths. Its narrow optical band gap of 0.79 eV makes it ideal for application in optoelectronic devices and solar cells, where efficient absorption of lower-energy photons is desirable. Morphological research utilizing field emission scanning electron microscopy (FESEM) revealed that HgS particles are polyhedral with surface imperfections. These properties improve ion transport and access to active areas, resulting in higher energy densities and faster charge/discharge rates.

Energy-dispersive X-ray spectroscopy (EDX) verified the presence of mercury and sulphur, thereby verifying the material's chemical constitution. The combination of these beneficial characteristics makes HgS an attractive electrode material for ECs. Its extensive optical absorption and good morphological properties contribute to its promise in advanced energy storage technologies.

Finally, the outcomes of this study provide the path for future improvement and development of HgS-based capacitors. Future research should concentrate on improving the synthesis process, increasing material stability, and investigating practical applications to fully realize HgS's potential in real-world energy storage systems. This study establishes a solid platform for intriguing developments in next-generation electrochemical capacitors by combining fundamental electrochemical concepts with comprehensive morphological characterization.

ACKNOWLEDGEMENT

The contributors warmly credit Prof. Anand Srivastava, Hon. Vice Chancellor of Netaji Subhas University of Technology, for providing infrastructural resources.

DECLARATION OF COMPETING INTEREST

It is declared that this article is original and written by the stated authors. There is no conflict of interest between the authors.

CONFLICTS OF INTEREST OR COMPETING INTERESTS

No conflicts of interest exist among the authors.

DATA AND CODE AVAILABILITY

All the data is presented in the manuscript and no supplementary data is needed.

REFERENCE

- [1] Shreya, P. Phogat, R. Jha, and S. Singh, "Electrochemical study of cerium and iron doped MoO₃ nanoparticles showing potential for supercapacitor application," *Next Materials*, vol. 5, p. 100260, Oct. 2024, doi: 10.1016/J.NXMATE.2024.100260.
- [2] P. Phogat, D. Kumari, S. S.-P. Scripta, and undefined 2023, "Fabrication of tunable band gap carbon-based zinc nanocomposites for enhanced capacitive behaviour," *iopscience.iop.org*, Accessed: Jul. 07, 2024. [Online]. Available: <https://iopscience.iop.org/article/10.1088/1402-4896/acf07b/meta>
- [3] P. Phogat, R. Jha, S. S.-J. of P. and C. of Solids, and undefined 2024, "Electrochemical analysis of hydrothermally synthesized 2D/1D WS₂/WO₃ nanocomposites for solar cell application," *Elsevier*, Accessed: Jul. 07, 2024. [Online]. Available: <https://www.sciencedirect.com/science/article/pii/S0022369724002452>
- [4] P. Phogat, Shreya, R. Jha, and S. Singh, "Supercapacitive studies of hybrid materials based on cadmium deuterioxide chloride (CdDOCl) with activated carbon," *J Mater Sci*, 2024, doi: 10.1007/S10853-024-09874-0.
- [5] P. Phogat, R. Jha, S. S.-N. Materials, and undefined 2024, "Synthesis and characterization of C@ CdS core-shell structures for high-performance capacitors," *Elsevier*, Accessed: Jul. 07, 2024. [Online]. Available: <https://www.sciencedirect.com/science/article/pii/S2949822824001436>
- [6] D. Lau, N. Song, C. Hall, Y. Jiang, S. L.-... T. Energy, and undefined 2019, "Hybrid solar energy harvesting and storage devices: The promises and challenges," *Elsevier*, Accessed: Jul. 07, 2024. [Online]. Available: <https://www.sciencedirect.com/science/article/pii/S2468606919300498>
- [7] S. P. S. Badwal, S. S. Giddey, C. Munnings, A. I. Bhatt, and A. F. Hollenkamp, "Emerging electrochemical energy conversion and storage technologies," *Front Chem*, vol. 2, no. SEP, 2014, doi: 10.3389/FCHEM.2014.00079/FULL.
- [8] D. Sadiq *et al.*, "Review of Energy Storage Systems in Regenerative Braking Energy Recovery in DC Electrified Urban Railway Systems: Converter Topologies, Control Methods &," *techriv.org*, 2023, doi: 10.36227/techriv.16699942.v1.
- [9] P. Moseley, *Electrochemical energy storage for renewable sources and grid balancing*. 2014. Accessed: Jul. 08,

2024. [Online]. Available: https://books.google.com/books?hl=en&lr=&id=N0Z9AwAAQBAJ&oi=fnd&pg=PP1&dq=electrochemical+energy%2Brap+id+energy+delivery%2Bregenerative+braking%2Bautomobile+s%2Bpeak+power+shaving%2B+electrical+grids&ots=-6tObflUxs&sig=ivOFpH6L_hWYN7Op6x56kA8rELc
- [10] A. Burke, J. Z.-J. of E. Storage, and undefined 2021, "Past, present and future of electrochemical capacitors: technologies, performance and applications," *Elsevier*, Accessed: Jul. 07, 2024. [Online]. Available: <https://www.sciencedirect.com/science/article/pii/S2352152X21000736>
- [11] G. Yu, X. Xie, L. Pan, Z. Bao, Y. C.-N. Energy, and undefined 2013, "Hybrid nanostructured materials for high-performance electrochemical capacitors," *Elsevier*, 2012, doi: 10.1016/j.nanoen.2012.10.006.
- [12] J. M.-E. by F. B. and E. Fr and undefined 2013, "Market and applications of electrochemical capacitors," *Wiley Online Library*, Accessed: Jul. 07, 2024. [Online]. Available: <https://onlinelibrary.wiley.com/doi/pdf/10.1002/9783527646661#page=530>
- [13] K. Subramanya Bhat, J. Ganglbauer, E. Bosch, K. S. Bhat, J. Ganglbauer, and E. Bosch, "Techno-economic simulation and evaluation of scalable 'energy cells' locally generating renewable energy," *Springer*, vol. 139, no. 7, pp. 612–620, Nov. 2022, doi: 10.1007/s00502-022-01068-3.
- [14] D. Hubble, D. Brown, Y. Zhao, C. Fang, ... J. L.-E. &, and undefined 2022, "Liquid electrolyte development for low-temperature lithium-ion batteries," *pubs.rsc.org*, Accessed: Jul. 07, 2024. [Online]. Available: <https://pubs.rsc.org/en/content/articlehtml/2015/gz/d1ee01789f>
- [15] E. Mombeshora, V. N.-I. J. of Energy, and undefined 2015, "A review on the use of carbon nanostructured materials in electrochemical capacitors," *Wiley Online Library*, Accessed: Jul. 07, 2024. [Online]. Available: <https://onlinelibrary.wiley.com/doi/abs/10.1002/er.3423>
- [16] Y. Wang, Y. Song, Y. X.-C. S. Reviews, and undefined 2016, "Electrochemical capacitors: mechanism, materials, systems, characterization and applications," *pubs.rsc.org*, Accessed: Jul. 07, 2024. [Online]. Available: <https://pubs.rsc.org/en/content/articlehtml/2016/cs/c5cs00580a>
- [17] P. Phogat, R. Jha, S. S.-M. T. Sustainability, and undefined 2024, "Synthesis of novel ZnO nanoparticles with optimized band gap of 1.4 eV for high-sensitivity photo electrochemical detection," *Elsevier*, Accessed: Jul. 08, 2024. [Online]. Available: <https://www.sciencedirect.com/science/article/pii/S2589234724001593>
- [18] undefined Shreya, P. Phogat, R. Jha, S. S.-A. A. N. Materials, and undefined 2024, "Enhanced Electrochemical Performance and Charge-Transfer Dynamics of 2D MoS₂/WO₃ Nanocomposites for Futuristic Energy Applications," *ACS Publications*, vol. 7, no. 8, pp. 8593–8611, Apr. 2024, doi: 10.1021/acsanm.3c06017.
- [19] undefined Shreya, P. Phogat, R. Jha, S. S.-T. M. Chemistry, and undefined 2023, "Microwave-synthesized γ -

WO₃ nanorods exhibiting high current density and diffusion characteristics,” *Springer*, vol. 48, no. 3, pp. 167–183, Jun. 2023, doi: 10.1007/s11243-023-00533-y.

[20] J. Zhang, Z. Chen, Z. Wang, N. M.-M. research bulletin, and undefined 2004, “The synthesis of HgS microcrystallites with controllable structure and morphology,” *Elsevier*, vol. 86, no. 4, pp. 447–450, Mar. 2007, doi: 10.1007/s00339-006-3812-9.

[21] B. Patel, S. Rath, S. Sarangi, S. S.-A. P. A, and undefined 2007, “HgS nanoparticles: structure and optical properties,” *Springer*, vol. 86, no. 4, pp. 447–450, Mar. 2007, doi: 10.1007/s00339-006-3812-9.

[22] S. Yadav, R. Jha, P. Phogat, and S. Singh, “Preparation of Tin Oxide Nanoparticles via Co-Precipitation Method for its Future Applications,” *researchgate.net*, 2024, doi: 10.21275/MR24620131518.

[23] T. Jindal, P. Phogat, Shreya, S. Singh, and R. Jha, “Electrochemical and optical comparison of Cr³⁺, Co²⁺, Ag¹⁺, Hg¹⁺ and Pb⁴⁺ doped WO₃ as a thin layer working electrode for electrochemical sensing,” *Appl Phys A Mater Sci Process*, vol. 130, no. 7, Jul. 2024, doi: 10.1007/S00339-024-07666-6.

[24] S. Yadav, R. Jha, P. Phogat, and S. Singh, “Hydrothermal synthesis and characterization of tin telluride,” *RP Current Trends In Applied Sciences*, vol. 3, no. 1, pp. 2583–7486, 2024, Accessed: Jul. 08, 2024. [Online]. Available: https://www.researchgate.net/profile/Shreya-Sharma-77/publication/381006842_Hydrothermal_synthesis_and_characterization_of_tin_telluride/links/66594bb9479366623a3365a9/Hydrothermal-synthesis-and-characterization-of-tin-telluride.pdf

[25] P. Phogat, R. Jha, S. S.-M. S. and E. B, and undefined 2024, “Carbon nanospheres-induced enhanced capacitive dynamics in C/WS₂/WO₃ nanocomposites for high-performance electrochemical capacitors,” *Elsevier*, Accessed: Jul. 08, 2024. [Online]. Available: <https://www.sciencedirect.com/science/article/pii/S0921510724002198>

[26] S. Shreya, P. Phogat, ... S. S.-M. W. of, and undefined 2024, “Reduction mechanism of hydrothermally synthesized wide band gap ZnWO₄ nanorods for HER application,” *matec-conferences.org*, Accessed: Jul. 08, 2024. [Online]. Available: https://www.matec-conferences.org/articles/mateconf/abs/2024/05/mateconf_st_aar2023_01004/mateconf_staaar2023_01004.html

[27] Y. Tian *et al.*, “Mercury chalcogenide colloidal quantum dots for infrared photodetection: From synthesis to device applications,” *pubs.rsc.org*, Accessed: Jul. 08, 2024. [Online]. Available: <https://pubs.rsc.org/en/content/articlehtml/2023/nr/d2nr07309a>

[28] A. Sharma, P. Phogat, R. Jha, S. S.-N. Nanotechnology, and undefined 2024, “Electrochemical behavior of carbon/nickel sulfide nanocomposite thin films for advanced energy applications,” *Elsevier*, Accessed: Jul. 08, 2024. [Online]. Available: <https://www.sciencedirect.com/science/article/pii/S294982952400041X>

[29] T. S. Mathis, N. Kurra, X. Wang, D. Pinto, P. Simon, and Y. Gogotsi, “Energy storage data reporting in perspective—guidelines for interpreting the performance of electrochemical energy storage systems,” *Wiley Online Library*, vol. 9, no. 39, Oct. 2019, doi: 10.1002/aenm.201902007.

[30] A. Vlad, N. Singh, C. Galande, and P. M. Ajayan, “Design Considerations for Unconventional Electrochemical Energy Storage Architectures,” *Adv Energy Mater*, vol. 5, no. 19, Oct. 2015, doi: 10.1002/AENM.201402115.

[31] P. Phogat, R. Jha, S. S.-J. of P. and C. of Solids, and undefined 2024, “Electrochemical analysis of hydrothermally synthesized 2D/1D WS₂/WO₃ nanocomposites for solar cell application,” *Elsevier*, Accessed: Jul. 08, 2024. [Online]. Available:

<https://www.sciencedirect.com/science/article/pii/S0022369724002452>

[32] T. Kumar, P. Phogat, V. Sahgal, R. J.-P. Scripta, and undefined 2023, “Surfactant-mediated modulation of morphology and charge transfer dynamics in tungsten oxide nanoparticles,” *iopscience.iop.org*, Accessed: Jul. 08, 2024. [Online]. Available:

<https://iopscience.iop.org/article/10.1088/1402-4896/ace566/meta>

[33] Z. Kobos, “Electrochemical Impedance for Lab-on-a-chip Diagnostics,” 2019, Accessed: Jul. 08, 2024. [Online]. Available:

<https://search.proquest.com/openview/a14d97b2c0f644ce6547c4d2f03b5c84/1?pq-origsite=gscholar&cbl=18750&diss=y>

[34] P. Shinde, C. R.-M. C. Frontiers, and undefined 2021, “Advances in synthesis, properties and emerging applications of tin sulfides and its heterostructures,” *pubs.rsc.org*, Accessed: Jul. 08, 2024. [Online]. Available: <https://pubs.rsc.org/en/content/articlehtml/2020/qm/d0qm00470g>

[35] P. Phogat, A. Rai, Shreya, R. Jha, and S. Singh, “Effect of microwave, ultraviolet and ultrasonic treatment on crystal size and particle size of ZnS quantum dots as a working thin layer for solar cells,” *Indian Journal of Physics*, 2024, doi: 10.1007/S12648-024-03304-2.